Tandem High-Pressure Crystallography-Optical Spectroscopy Unpacks Noncovalent Interactions of Piezochromic Fluorescent Molecular Rotors

Alif N. Sussardi,[a] Gemma F. Turner,[b] Jonathan G. Richardson,[a] Mark A. Spackman,[b] Andrew T. Turley,[c] Paul R. McGonigal,[c,d]* Anita C. Jones[a]* and Stephen A. Moggach[b]*

[a] School of Chemistry, The University of Edinburgh, Edinburgh, EH9 3FL, United Kingdom

[b] School of Molecular Sciences, The University of Western Australia, Crawley, Perth, 6009, Australia

[c] Department of Chemistry, Durham University, Durham, DH1 3LE, United Kingdom

[d] School of Chemistry, The University of York, York, YO10 5DD United Kingdom

paul.mcgonigal@york.ac.uk; a.c.jones@ed.ac.uk ; stephen.moggach@uwa.edu.au

ABSTRACT: To develop luminescent molecular materials with predictable and stimuli-responsive emission, it is necessary to correlate changes in their geometries, packing structures, and noncovalent interactions with the associated changes in their optical properties. Here, we demonstrate that high-pressure single crystal X-ray diffraction can be combined with high-pressure UV-visible absorption and fluorescence emission spectroscopies to elucidate how subtle changes in structure influence optical outputs. A piezochromic aggregation-induced emitter, *sym*-heptaphenylcycloheptatriene (**Ph_7C_7H**), displays bathochromic shifts in its absorption and emission spectra at high pressure. Parallel X-ray measurements identify the pressure-induced changes in specific phenyl–phenyl interactions responsible for the piezochromism. Pairs of phenyl rings from neighboring molecules approach the geometry of a stable benzene dimer, while conformational changes alter intramolecular phenyl–phenyl interactions correlated with a relaxed excited state. This tandem crystallographic and spectroscopic analysis provides insight into how subtle structural changes relate to the photophysical properties of **Ph_7C_7H**, and could be applied to a library of similar compounds to provide general structure-property relationships in fluorescent organic molecules with rotor-like geometries.

Aromatic organic molecules with rotor-like geometries are promising solid-state fluorophores and possess flexible crystal structures that facilitate changes in their photophysical properties under a mechanical stimulus, known as mechanofluorochromism. The relative orientations and distances between π-surfaces (*i.e*. aromatic substituents) are well-established as important factors in controlling optoelectronic properties in solid-state devices, such as organic light-emitting diodes,[1-3] organic field-effect transistors,[4] optical storage components,[5-6] and photovoltaic cells.[7] Conformationally flexible fluorophores, such as molecular rotors, may display enhanced fluorescence in the solid state through so-called aggregation-induced emission (AIE) effects,[8-11] whereby non-radiative decay pathways through molecular motion are attenuated by geometric restrictions limiting the mobility of the molecule in the solid state.[12-13]

Beyond restricting intramolecular motions, solid-state packing can also impose specific noncovalent interactions and π-orbital overlap between neighboring molecules. These interactions may be advantageous, for example, by imparting strong electronic coupling and high charge mobility to acenes[14] or conjugated polymers[15] used in organic semiconductors, or they can be deleterious, for example by reducing the color purity of OLED materials.[16-17] Clearly, the manipulation and control of intermolecular interactions in the solid state is crucial to the design and optimization of functional organic solids.

Structure-property relationships in functional materials can be probed by deforming their structure under high-pressure. A single crystal can be compressed in a diamond anvil cell and its crystal structure and spectroscopic properties followed in situ.[18] This technique has been used to elucidate structure-property relationships in functional organic crystals with luminescence and negative linear optical properties,[19-20] inorganic complexes,[21-23] and flexible framework materials,[24-28] to name a few.

Phenyl-substituted organic molecules with rotor-like geometries, such as sym-pentaphenylcyclopentadiene (**Ph_5C_5H**) and sym-heptaphenylcycloheptatriene (**Ph_7C_7H**, Figure 1), are archetypal fluorescent solids, and possess sterically-

cluttered geometries that afford inefficient crystal packing that is susceptible to deformation under pressure.[29-34] Under ambient conditions, their hindered structure prevents significant motion of the locally emissive phenyl groups and inhibits the formation of short, stacked π–π interactions between proximal phenyl substituents, typically resulting in short-wavelength fluorescence emission in the violet or blue region.[35] Under applied pressure, the fluorescence emission usually red-shifts as the π–π interactions are forced closer together.[29-31] High-resolution structural characterization of the intramolecular and intermolecular aromatic interactions during compression is necessary to understand the mechanofluorochromic response of these compounds.

Crystals of phenyl-substituted organic molecules are predominantly cohered through intramolecular and intermolecular phenyl dimers, with either displaced-stacked (π–π) or T-shaped (CH–π) conformations.[36-39] The stability of interactions can be inferred by comparing their geometries to the theoretically most stable co-conformations of two benzene molecules, quantified by the distance between phenyl centroids (*C*), the distance between a phenyl centroid and the plane of interacting phenyl ring (*P*), the angle between phenyl ring planes (∠), and the displacement of the phenyl rings from one another (*d*), illustrated in Figure 2.[36] Under ambient conditions, benzene forms a T-shaped interaction with the parameters: *C* = 5.01 Å, *P* = 4.92 Å, ∠ = 75.4° and *d* = 0.945 Å, and a displaced-stacked conformer with parameters of *C* = 3.95 Å, *P* = 3.54 Å, ∠ = 0° and *d* = 1.752 Å. [36]

A previous report on the fluorescent properties of hexaphenylbenzene and its homologues of varying central ring size (cyclopropene, cyclopentadiene and cycloheptatriene) demonstrated that the fluorescence emission wavelength depends upon three factors in the crystalline phase: (i) the extent of interdigitation of the phenyl substituents in the crystal, (ii) the size of the cyclical core and (iii) the conformational flexibility of the molecule, all of which dictate the intermolecular and intramolecular interaction inter-phenyl interactions in the crystal.[35, 40] The increased conformational freedom of the seven-membered core in **Ph_7C_7H** (*Figure 1*),[41] together with the out-of-plane bond angles provided by the aliphatic carbon center in the ring, permits the formation of an intramolecular, transannular T-shaped phenyl dimer (involving Ph^3 and Ph^7, *Figure 1*), which gives rise to fluorescence from a relaxed excited state. Computed structures of the excited state show a shortened transannular inter-phenyl interaction compared with the ground state structure, demonstrating the importance of the flexibility of the central ring to the photophysical properties of these systems.[35]

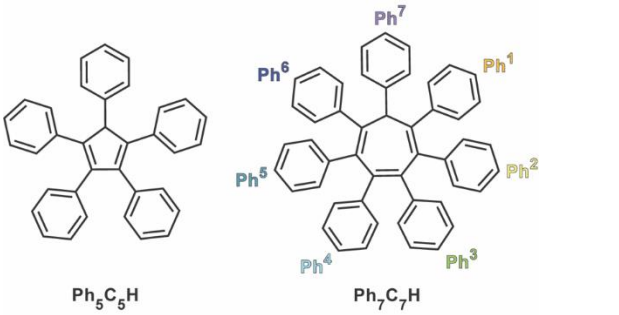

Figure 1. Structural formulas of **Ph_5C_5H** and **Ph_7C_7H**.

Organic rotors are attractive systems for optoelectronic devices because their fluorescence output can be controlled, both by synthetic design[42-44] and under a mechanical stimulus[29-34] (*e.g.* compression,[45-47] grinding,[48] scraping[49] *etc*.). Pronounced changes in the fluorescence output typically accompany large structural deformations in the crystal, such as conformational isomerism,[29, 47, 50] polymorphism[51] or amorphisation.[52] However, subtle changes to the structure of the emissive state, such as slight compression of the intermolecular aromatic interactions or small distortions to the molecular geometry, may also result in detectable mechanofluorochromism.[53-54]

The ability to tune the fluorescent output of solids benefits numerous technological applications. However, the structure–fluorescence relationships in organic rotors are underdeveloped, limiting the synthesis of bespoke fluorophores with predictable and tunable fluorescence. Recently, Yu, Gao, and Gu have reported high-pressure photophysical measurement of AIE materials supported by angle-dispersive X-ray diffraction to measure changes in unit cell dimensions.[55-5656] Here, we monitor structural changes at the molecular level, correlating precise changes in molecular geometry and intermolecular distances with optical properties of AIE materials through a combination of atomically resolved X-ray crystallographic measurements and electronic spectroscopy under high pressure. We examine the structure-fluorescence relationships in **Ph_7C_7H** by tandem single crystal X-ray diffraction, fluorescence emission spectroscopy and UV-visible absorption spectroscopy measurements under high hydrostatic pressure conditions. The effect of pressure on specific dimeric interactions of phenyl groups (both intermolecular and intramolecular) are correlated with pressure-induced shifts in the absorption and emission spectra and rationalized by theoretical calculation of the pairwise intermolecular interaction energies between the **Ph_7C_7H** molecules in the crystal.

The photophysical properties of **Ph_5C_5H**, (*Figure 1*), which does not feature any intramolecular T-shaped inter-phenyl interactions, are also examined to distinguish the spectral effects of increased intermolecular interactions from those due

to the intramolecular dimer interaction in **Ph_7C_7H**. However, crystallographic data could not be obtained for **Ph_5C_5H** due to its poor crystallinity.

Upon compression of **Ph_7C_7H** to ~3 GPa, bathochromic shifts in both its absorption and emission spectra occur, resulting from enhancement of the intermolecular phenyl–phenyl interactions at high-pressure. Conformational distortion of the molecule in this pressure region also enhances an intramolecular phenyl–phenyl interaction, causing the molecule to adopt a ground-state geometry approaching that predicted for the relaxed excited state.[35] At pressures above 2 GPa, the structures of intermolecular phenyl dimers become close to the equilibrium geometry of the displaced-stacked (DS) benzene dimer, resulting in bathochromic excimer emission. Excitonic interactions in these closely stacked phenyl dimers cause increased absorption at longer wavelengths, shifting the absorption from the UV into the blue region, causing a reversible, piezochromic color change of the crystal from colorless to yellow. These data not only demonstrate the stimulus-responsive behavior of this particular molecular rotor, but also establish that tandem high-pressure crystallography–optical spectroscopy provides rich structure–fluorescence relationships for emitting crystals. Although only a single system is examined here, applying this method more broadly to other organic materials may lend insights into how subtle changes in π-orbital orientation and overlap can be used to tune and optimize optoelectronic properties.

RESULTS AND DISCUSSION

Ph_7C_7H under Ambient Conditions

Under ambient conditions, **Ph_7C_7H** crystallizes in the triclinic space group, $P\bar{1}$. Two molecules occupy the unit cell and are arranged about the inversion center such that the phenyl substituents are interdigitated (*Figure 2a*). Similar interdigitated motifs envelop the molecules in all directions, with proximal pairs of phenyl substituents coupling through either T-shaped (T) aromatic interactions (edge-to-face) or displaced-stacked (DS) aromatic interactions (staggered face-to-face, *Figure 2b*). Five unique T intermolecular interactions (labelled $T_{1\text{-}3}$ $T_{3\text{-}1}$, $T_{4\text{-}6}$ and $T_{4\text{-}6}$, $T_{6\text{-}4}$ and $T_{7\text{-}3}$) and two unique DS intermolecular interactions (labelled $D_{5\text{-}5}$, and $D_{3\text{-}6}$) exist, together with the transannular, intramolecular T interaction ($T_{7\text{-}3\text{intra}}$ *Figure 2c*) identified previously.[35] The strength of the phenyl–phenyl interaction can be assessed by comparing the conformation of the phenyl pair to the known structures of the noncovalent dimer of benzene.[36]

In **Ph_7C_7H**, the phenyl–phenyl interactions are comparatively weak with only one of the phenyl pairs approaching a stable dimer structure, which is an intermolecular T interaction ($T_{7\text{-}3}$) (*Table S9*). In contrast, the **Ph_5C_5H** homologue (which has no intramolecular T interactions) features two intermolecular DS interactions (labelled $D_{4\text{-}4}$ and $D_{3\text{-}3}$ in *Supplementary Figure S4 and Table S5)* that are close to the equilibrium geometry of the DS benzene dimer. Here, the coordinates for **Ph_5C_5H** from the previously published crystal structure (Cambridge Structural Database reference: 'KUKDEZ')[57-58] was used to identify significant intermolecular interactions. These dimer structures are of spectroscopic interest as they are precursors for excimer formation. Benzene itself forms excimers, with characteristic broad, bathochromic emission, in the gas[59] and liquid phases,[60] but in the crystal, where nearest neighbors are in a T arrangement,[61] formation of the parallel, stacked excimer conformation cannot occur.[8]

The differing phenyl–phenyl interactions present in **Ph_7C_7H** and **Ph_5C_5H** are manifested clearly in their optical spectra. For crystals of **Ph_7C_7H**, the wavelength of the absorption spectrum red-edge (*Figure 3a*) matches the absorption spectrum in solution reported by Sturala *et al*.,[35] consistent with the absence of any significant, intermolecular, excitonic interactions, whereas, for **Ph_5C_5H** (*Table S17* and *Figure S8*) the absorption red-edge (408 nm) is considerably red-shifted (>2000 cm^{-1}) relative to that of the solution-phase spectrum (375 nm),[62] as a result of the DS dimer interactions. The emission spectrum of **Ph_7C_7H** (*Figure 3b*) coincides with the solution-phase spectrum reported previously.[35]

The sizeable Stokes shift (3300 cm^{-1}) between absorption red-edge and emission maximum can be attributed to conformational relaxation of the intramolecular transannular phenyl dimer ($T_{7\text{-}3\ \text{intra}}$, *Table S8*) in the excited state, prior to emission. The similarity between the spectra in the crystalline state and those in solution-phase confirms that the Stokes shift is due to conformational change rather than solvent relaxation. The emission of **Ph_5C_5H** (*Figure S8)* is substantially red-shifted (by ~1900 cm^{-1}) relative to solution-phase,[35] and shows a Stokes shift of ~3100 cm^{-1}, indicative of excimer formation. Relaxation of the initially excited (Franck–Condon) DS dimer structure to form an excimer requires shortening of the inter-planar distance by approximately 0.4 Å during the excited-state lifetime.[63] In crystalline pyrene, a similar structural relaxation during excimer formation has been observed to occur on the picosecond timescale.[64]

Photophysical Properties of Ph_7C_7H at High-Pressure

The photophysical properties of **Ph_7C_7H** change in response to the application of high-pressure, as the phenyl–phenyl aromatic interactions in the crystal are enhanced. The UV-visible absorption red-edge shifts gradually from 359 nm at ambient pressure to 379 nm at 3.06 GPa (*Figure 3a and Figure 3c*), a bathochromic shift of 1470 cm^{-1}. Above 1.13 GPa, the absorption peak broadens and develops an increasingly intense long-wavelength tail, with increasing pressure. The change in spectral profile at higher pressures can be linked to the formation of DS intermolecular interactions with structures resembling the equilibrium geometry of the benzene dimer, as discussed below. Unlike **Ph_5C_5H**, where DS π-π interactions are already present at ambient pressure (*vide supra*), these interactions only develop at high pressure in **Ph_7C_7H**. Above 2.65 GPa, piezochromism is evident by eye; the crystal changes from colorless to yellow (*Figure 3c* and *Figure S1*) as the absorption spectrum shifts from the UV into the blue.

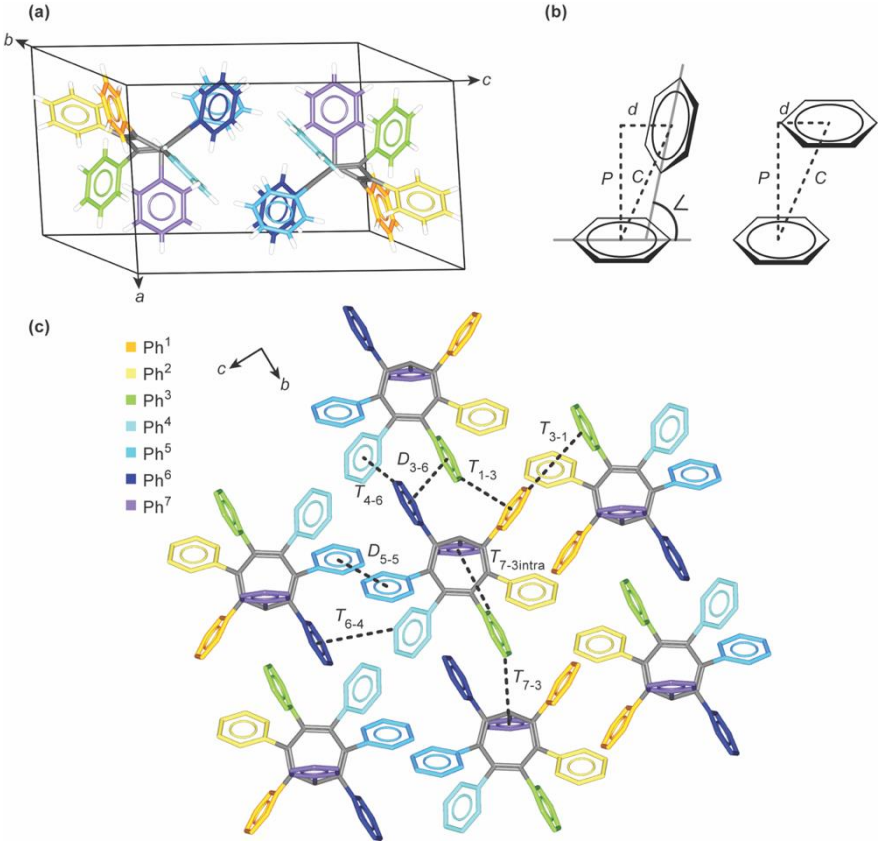

Figure 2. (a) Stick representation of the **Ph_7C_7H** molecules in the triclinic unit cell ($P\bar{1}$, a = 9.8539 (2) Å, b = 10.0192 (2) Å, c = 19.1805 (4) Å, α = 92.256 (2)°, β = 90.447 (2)°, γ = 108.563 (2)°, V = 1793.33 (7) $Å^3$). Phenyl substituents are labelled and colored according to their position on the cycloheptatriene ring. **(b)** Parameters used to define the conformations of aromatic dimers. **(c)** Phenyl–phenyl interactions, T ($T_{n\text{-}m}$, where n corresponds to the top-bar of the T pair) and DS ($D_{n\text{-}m}$), in a cluster of **Ph_7C_7H** molecules in the crystal under ambient conditions. Hydrogen atoms are omitted for clarity. Interphenyl geometric parameters are given in *Tables S8 – S15*).

At pressures up to 2.12 GPa, the wavelength of fluorescence (*Figure 3b and Figure 3c*) shows little change with increasing pressure, in contrast to the progressive bathochromic shift of the absorption spectrum. This is consistent with structural relaxation in the excited state and implies that the structure of the relaxed emitting species is essentially unaffected by compression. The decrease in Stokes shift (*Table S16*) shows that, as the pressure is increased, the ground-state (Franck–Condon) geometry more closely resembles that of the emitting state. At pressure above 1.82 GPa, a shoulder becomes apparent on the long-wavelength side of the fluorescence maximum (*Figure 3b*). The intensity of this shoulder increases with increasing pressure, leading to a bathochromic shift in the emission maximum above 2.65 GPa (*Figure 3c*). The change in the emission spectral profile correlates with the broadening of the absorption spectrum,

indicating that the long-wavelength emission is linked to the excitation of DS phenyl–phenyl dimers that are capable of excimer formation.

The intensity of the emission maximum increases with increasing pressure up to 2.65 GPa (*Figure S9*). However, this is not due to the influence of intermolecular interactions on quantum yield (aggregation-induced emission) but arises from the increase in absorbance at the excitation wavelength (365 nm) as a result of the pressure-induced red shift in the absorption spectrum (*Figure 3a*). There is a linear correlation of fluorescence intensity with the relative absorbance, up to 2.65 GPa (*Figure S10*), indicating a pressure-independent quantum yield. At 3.03 GPa, there appears to be a decrease in the quantum yield, corresponding to an increase in the contribution from long-wavelength emitting excimers.

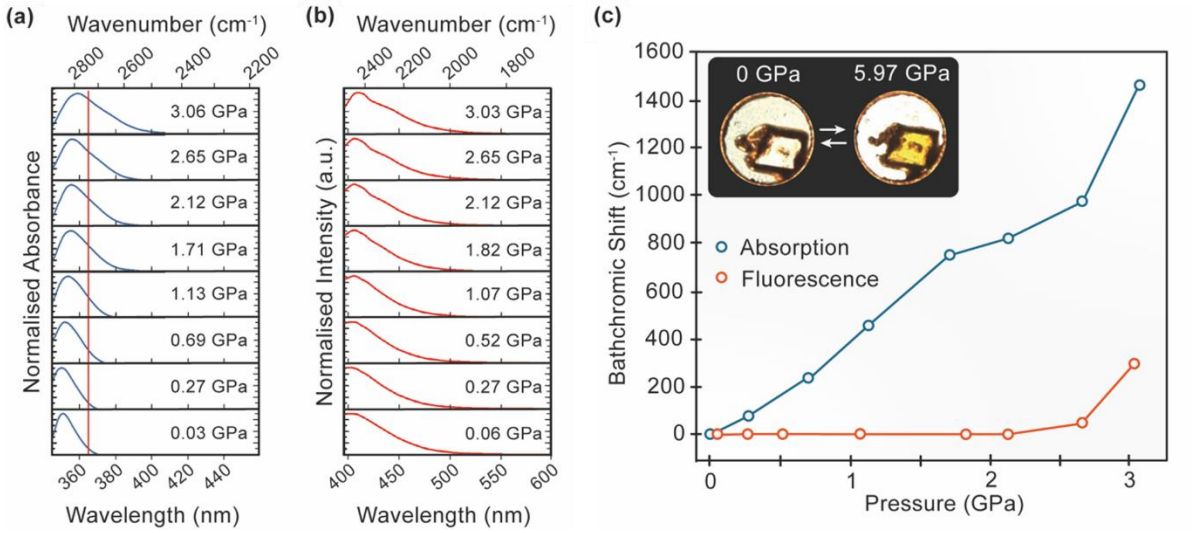

Figure 3. (a) High-pressure UV-visible absorption spectra (vertical red line indicates the fluorescence excitation wavelength of 365nm) and **(b)** high-pressure fluorescence emission spectra for **Ph_7C_7H** (365 nm excitation wavelength). **(c)** Bathochromic shift in UV-visible absorption red edge (blue line) and fluorescence emission maximum (red-orange line) of a single crystal of **Ph_7C_7H** during hydrostatic compression. The bathochromic shift in the UV-visible absorption spectrum results in reversible piezochromism of the crystal from colorless (ambient pressure) to yellow (6.0 GPa) (inset).

Structure of Ph_7C_7H at High-Pressure

To determine the origin of the evolution of the absorption and emission spectra of **Ph_7C_7H** at high-pressure, pressure-induced changes to the crystal structure are examined (*Figure 4)*. Diffraction experiments were performed on a separate crystal of Ph7C7H in a newly loaded diamond anvil cell. As previously mentioned, the crystal structure of **Ph_5C_5H** could not be assessed at high-pressure due to inadequate crystal quality. Crystallographic data for **Ph_7C_7H** are given in *Tables S1* and *S2*, and unit cell dimensions are given in *Table S3*. Atomistic structures could only be obtained to 2.61 GPa due to broadening of the Bragg reflections and lowering of the diffraction resolution between 3.09 GPa and 4.90 GPa, followed by amorphization by 5.97 GPa. This behaviour above 2.61 GPa could be caused by the sample reaching the hydrostatic limit of the pressure-transmitting medium, though further studies would be required to confirm this.

Upon compression of **Ph_7C_7H** from ambient pressure to 3.1 GPa, the unit cell volume contracts by 322.1 (9) $Å^3$ (−18.0%) (*Figure 4a*), corresponding to an isothermal bulk modulus, K_0, of 4.9(13) GPa (*Supplementary Information S4*). Compression of the unit cell is anisotropic, with the *a*-, *b*- and *c*-axes shortening by 0.403 (2) Å (-4.1%), 0.436 (2) Å (-4.4%) and 1.766 (6) Å (-9.2%), respectively. The most compressible axis (the *c*-axis) is aligned with pairs of molecules whose phenyl substituents are efficiently interdigitated, while the less compressible *a*- and *b*-axes are coincident with less complementary phenyl packing arrangements. From calculation of the principal axes in **Ph_7C_7H** (*Table S4*),[65] the most compressible direction is coincident with the transannular $T_{7\text{-}3intra}$ and intermolecular $T_{7\text{-}3}$ dimers ([2 -1 0], 97(29) TPa^{-1}), while the least compressible is approximately aligned with $T_{6\text{-}4}$ and $T_{4\text{-}6}$ ([0 5 1], 22.8(2) TPa^{-1}).

Compression of the unit cell volume between ambient pressure and 2.6 GPa deforms the conformational geometry of **Ph_7C_7H** (*Figure 4b*). Between ambient pressure and 2.6 GPa, the molecule appears to 'fold', quantified by a decrease in

the angle subtended between the phenyl substituent at the sp^3 center in the cycloheptatriene ring, Ph^7, and the C7 and C3 atoms in the cyclical core, θ, by 3.7° (*Figure 4b*). This deformation shortens the intramolecular, transannular interaction, $T_{7\text{-}3intra}$ (*Figure 2c*, *Table S8*), bringing the centroids of Ph^7 and Ph^3 substituents closer together by 0.33 (2) Å (−6.5%). As pressure increases, the molecule adopts a geometry more closely resembling that of the excited state predicted by density functional theory in a previous study.[35] This is consistent with the observed decrease in Stokes shift with increasing pressure.

The broadening of the absorption and emission spectral profiles to longer wavelengths at pressures above 2.12 GPa results from compression of DS intermolecular phenyl dimers (*Figure 2c and Figure 5, Tables S10 and S11*), which facilitates excimer formation. Interaction $D_{3\text{-}6}$ (*Figure 5*, *Table S10*) appears to be most the important to the piezochromism and pressure-induced excimer emission of this system due to its close approach to the benzene dimer structure under applied pressure. At ambient pressure, the $D_{3\text{-}6}$ interplanar distance and angle are already close to those of the benzene dimer,[36] but the displacement is much greater (*C* = 4.777 Å, *P* = 3.488 Å, *d* = 3.264 Å, ∠ = 2.06°, *Table S10*). Upon increasing the pressure above 1.59 GPa, the displacement approaches the equilibrium distance in the benzene dimer (1.74 Å), decreasing by 33% to around 2 Å (*C* = 4.074 Å, *P* = 3.505 Å, *d* = 2.077 Å, ∠ = 15.99° at 2.61 GPa, *Table S10*), enabling excimer formation.[66] Even at high pressure, the crystal structure is able to relax locally around the excited molecule to attain an excimer geometry within the excited state lifetime. However, the continued presence of shorter-wavelength, monomer-like fluorescence suggests that emission occurs from a range of structures on the relaxation pathway between the Franck–Condon geometry and the lowest energy, excimer state.

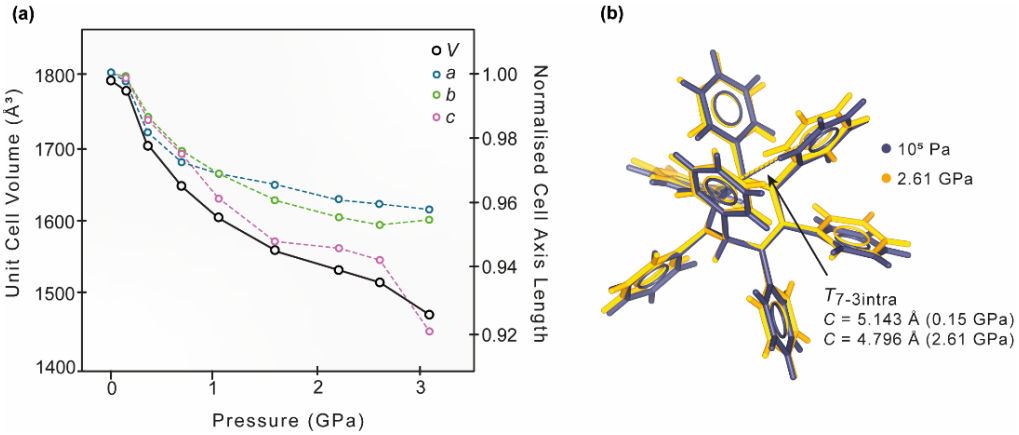

Figure 4. (**a)** Unit cell volumes and normalized unit cell axis lengths of **Ph_7 C_7H** as a function of hydrostatic pressure. Error bars are within the data point markers. (**b)** Overlay of the structure of **Ph_7 C_7H** at ambient pressure (purple) and 2.61 GPa (yellow) showing the conformational change of the molecule with pressure and shortening of the intramolecular interaction, $T_{7\text{-}3intra}$.

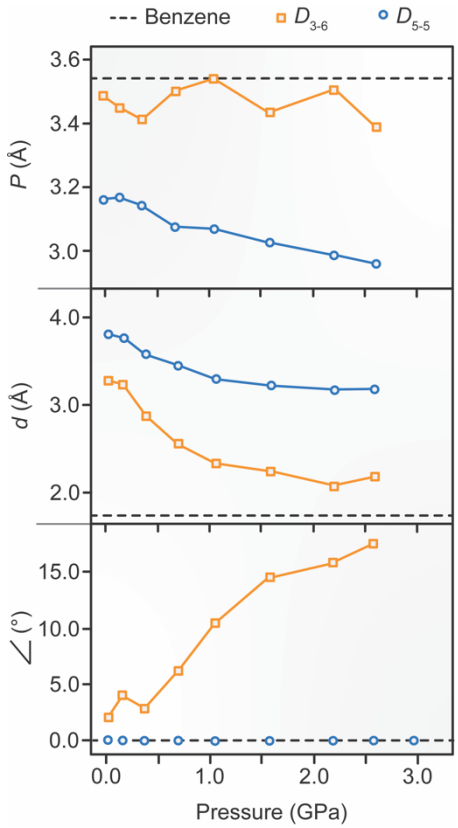

Figure 5. Phenyl–phenyl conformation structural parameters of the intermolecular DS phenyl dimers in **Ph_7C_7H** as a function of pressure. The values for the equilibrium geometry of the benzene dimer are shown for comparison.

The D_{5-5} interaction (*Figure 5* and *Table S9*) is also significantly enhanced with increasing pressure, with the displacement, *d*, decreasing by 16% between ambient pressure and 2.61 GPa (from (*C* = 4.927 Å, *P* = 3.161 Å, *d* = 3.779 Å, ∠ = 0° to (*C* = 4.334 Å, *P* = 2.957 Å, *d* = 3.169 Å, ∠ = 0°, *Table S11*), which may contribute to bathochromic spectral shifts, since increase in displaced-stacked interactions is commonly associated with decreased excitation energy.[29-31] However, the displacement remains greater than 3 Å making excimer formation unfavorable.[36, 67] Compression of the intermolecular tilted T interactions (*Figure 2c*) are not thought to be significant in the pressure-dependence of the photophysical properties of **Ph_7C_7H**. However, they are important to the structural stability of the crystal and its response to pressure. Under ambient conditions, the T_{7-3}, T_{6-4} and T_{4-6} dimers most closely resemble the equilibrium T dimer of benzene (*Tables S9*, *S12* and *S13*), suggesting that these are the most stable. T_{7-3} closely resembles the benzene dimer at pressures below 1.05 GPa, before increasingly deviating from the equilibrium benzene geometry as pressure in increased to 2.61 GPa (*Table S9*).[36]

Upon compression, T_{6-4} and T_{4-6} are enhanced, with T_{4-6} becoming essentially identical to the benzene dimer at pressures above 1.59 GPa. (*Tables S12* and *S13*). The T dimers, $T_{7-3intra}$ and T_{3-1} (*Tables S8* and *S15*) are comparatively unimportant to the crystal stability, with conformations under both ambient and high-pressure conditions divergent from those found in dimeric benzene.[36] T_{1-3} (*Table S14*) is insignificant at ambient pressure but becomes similar to the benzene dimer when the pressure exceeds 1.59 GPa. All the T-shaped intermolecular interactions are highly compressible, undergoing changes in lateral displacement by as much as 60% (T_{1-3}) between ambient pressure and 2.61 GPa, contributing to the high compressibility of the crystal.

Pairwise Interactions between Molecules in Ph_7C_7H at High-Pressure

The intermolecular interactions affecting the stability and compressibility of **Ph_7C_7H** were assessed by calculation of the pairwise molecule-to-molecule intermolecular interaction energies in the crystal using CrystalExplorer (CE-B3LYP functional).[68-69] Changes to the internal energy of the **Ph_7C_7H** molecule as its conformation deforms under pressure are

also expected to occur but are not assessed here nor are the focus of this discussion. A total of nine stabilizing pairwise intermolecular interactions were found within a cluster of molecules within a diameter of ~14 Å, which are labelled in order of decreasing interaction strength from 1 to 9 (*Figure 6* and *Supplementary Figure S11*). Under ambient conditions, the total interaction energies are between −50 kJ·mol^{-1} and −17 kJ·mol^{-1}. They are dominated by dispersion and repulsion terms with a significant electrostatic component (*Supplementary Information S7*). The pairwise interactions are shown in *Figure 6a–c* and *Tables S18–27*.

The two strongest interactions, 1 (E_{total} = −50 kJ·mol^{-1}) and 2 (E_{total} = −42 kJ·mol^{-1}), form between alternating pairs of efficiently interdigitated **Ph$_7$C$_7$H** molecules along the crystallographic *c*-axis, with inter-centroid distances of 9.8 Å and 10.2 Å, respectively, at ambient pressure (*Figure 6a*, *Tables S18* and *S19*). Weaker interactions with total energies between −35 kJ·mol^{-1} to −17 kJ·mol^{-1} form between the less efficiently interdigitated molecules along the crystallographic *a*- and b-axes of the cluster, with inter-centroid distances between 9.9 Å and 12.8 Å.

The stability of organic, aromatic hydrocarbons is most likely governed by dispersion with smaller contributions from the electrostatic and polarization components of the aromatic interactions.[70-71] From comparison of the T and DS interactions in **Ph$_7$C$_7$H**, T dimers appear to be more important to interaction stability. This observation is unsurprising since the T dimers are more numerous than the DS interactions and have more optimal conformational geometries at ambient pressure. However, it is an important consideration for crystal engineering compounds with predictable pressure-responsive photophysical properties as it indicates that T dimers are likely to govern the stability of the crystal under pressure and, by extension, the compressibilty of DS dimers that dictates the photophysical response of the system.

The strongest pairwise interaction, 1, features three dimers with conformations close to equilibrium benzene dimers, $T_{4\text{-}6}$, $T_{6\text{-}4}$ and $D_{5\text{-}5}$, accounting for its high stability. The second strongest pairwise interaction features $T_{1\text{-}3}$ and $T_{3\text{-}1}$, which is unexpected since these dimers do not have optimal conformations at ambient pressure. However, this molecular pair has a large dispersion contribution under ambient conditions (E_{dis} = −58.3 kJ·mol^{-1} for interaction 2 compared with E_{dis} = −64.3 kJ·mol^{-1} for interaction 1; *Figure 6a*, *Tables S18* and *S19*). Interaction 3, which features $D_{3\text{-}6}$, has a short distance between molecular centers of 10 Å (*i.e.* the distance between the center of one molecule to the center of another), leading to considerable dispersion forces (*Figure 6b*, *Table S20*). The remaining interactions feature less stable T-shaped dimers and are not discussed in detail here.

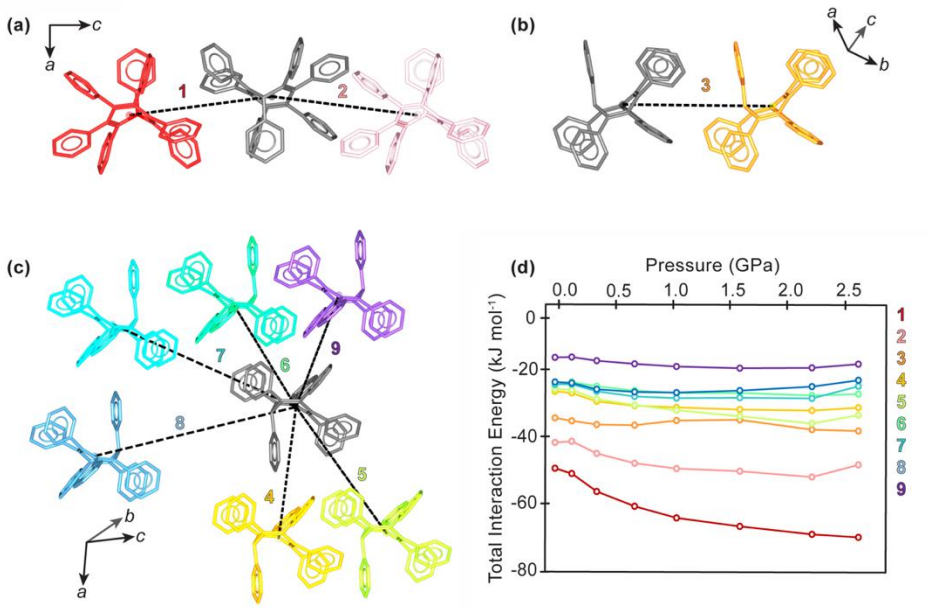

Figure 6. (a) Pairwise intermolecular interactions 1 (red) and 2 (pink) between **Ph$_7$C$_7$H** molecules at ambient pressure. **(b)** Pairwise intermolecular interaction 3 (red-orange) at ambient pressure. **(c)** Pairwise intermolecular interactions 4 (yellow-orange), 5 (yellow-green), 6 (blue-green), 7 (cyan), 8 (light-blue) and 9 (purple) at ambient pressure. **(d)** Plot of total interaction energy for the nine strongest interactions between pairs of **Ph$_7$C$_7$H** molecules in a ~14 Å-diameter cluster as a function of applied hydrostatic pressure.

Changes to the interaction strength between pairs of molecules under applied pressure is informative of the thermodynamic factors driving deformation of the crystal. It is known that displaced-stacked interactions are the most important to piezochromism and mechanofluorochromism in fluorescent organic crystals,[29-31] so pairwise interactions 1 and 3 in **Ph_7C_7H** are presumably the important to piezochromism and mechanofluorochromism of **Ph_7C_7H** since they feature DS interactions.

During compression from ambient pressure to 2.6 GPa, interaction 1 is gradually stabilized by −20 kJ·mol^{-1} (*Figure 6d*), consistent with the substantial enhancements of $T_{4\text{-}6}$, $T_{6\text{-}4}$. There is also likely to be significant dispersion forces between CH groups as the distance between the molecule centroids decreases from 9.8 Å to 8.8 Å, which is the shortest in the crystal. By contrast, interaction 3 exhibits only slight stabilization by −4 kJ·mol^{-1} during compression, reflecting little influence of the enhancement of $D_{3\text{-}6}$ interaction on overall stability. This highlights the unimportance of the photophysically-relevant DS interactions to the stability of the crystal.

Interaction 2 shows the second largest stabilization between ambient pressure and 2.6 GPa, becoming stabilised by approximately −7 kJ·mol^{-1}, which is consistent with significant enhancement of the $T_{3\text{-}1}$ and $T_{1\text{-}3}$. All remaining pairwise interactions exhibit the same trend of slight stabilization up to pressures of 1.1 GPa – 1.6 GPa, as dispersion forces increase, before slight destabilization with increasing pressure up to 2.6 GPa as the repulsive contribution becomes dominant, leading to partial loss of crystallinity above this pressure.

These results demonstrate that structure of the T dimers should be considered when designing fluorescent organic crystals, since they are more important to its structural response to pressure, which in turn affects the compressibility of the DS interactions.

CONCLUSIONS

The development of organic crystals with bespoke optoelectronic properties and stimuli-responsive behavior benefits a diverse range of applications but is hindered by the lack of established design principles. In this work, we have demonstrated that the effects of high pressure on optical spectra can be correlated with specific changes in molecular conformations and packing structures.

We have found that the fluorescence wavelength and color of the crystal of a classical, phenyl-substituted organic rotor, **Ph_7C_7H**, can be tuned by compression of the DS phenyl dimers under applied pressure, which shorten under pressure and adopt configurations closer to that of the equilibrium displaced-stacked conformer of benzene dimer, which is thought to increase the excitonic interaction between the phenyl substituents, thereby lowering the transition energy between the ground and excited state and enabling relaxation to an excimeric state. However, the T-shaped inter-phenyl dimers are more important to the stability of the crystal under pressure (in addition to dispersion forces in general), which is likely to be relevant to crystal engineering of fluorescent organic rotors in general. It is notable that the fluorescence properties of the molecular rotor are strongly influenced by excited-state structural relaxation, even in the solid state. While the absorption spectrum shifts steadily to longer wavelength with increasing pressure, the wavelength of emission from the relaxed excited-state molecular structure remains essentially constant, until pressures are reached where enhanced intermolecular phenyl–phenyl interactions result in excimeric emission, enabled by relaxation of the local crystal structure. Since aromatic interactions are pervasive in fluorescent organic crystals and the formation of phenyl dimers is particularly common in rotor-type systems, it is expected that the structure–fluorescence dependence reported here will be applicable to similar fluorescent systems.

Overall, this work demonstrates the piezobathochromic behavior of a classical organic rotor and draws explicit connections between its structural and optical properties. High-resolution structural analysis in tandem with interaction energy calculations and photophysical measurements enables the changes in the intermolecular interactions and molecular geometry to be related to the optoelectronic properties, providing a better understanding of functional organic materials in the solid state.

AUTHOR INFORMATION

Corresponding Author

Dr Paul R. McGonigal (paul.mcgonial@york.ac.uk); Prof Anita C. Jones (a.c.jones@ed.ac.uk); Prof Stephen A. Moggach (stephen.moggach@uwa.edu.au)

Author Contributions

S.A.M., A.C.J. and P.R.M. conceived the idea. A.N.S. and A.C.J. devised and performed the fluorescence emission and UV-visible spectroscopy experiments and A.N.S., G.F.T, S.A.M. collected and refined the crystal structures. All authors contributed to analyzing the data and writing the manuscript.

Funding Sources

Any funds used to support the research of the manuscript should be placed here (per journal style).

Notes

Australian Research Council (ARC)
Engineering and Physical Sciences Research Council (EPSRC)

ACKNOWLEDGMENT

A.N.S acknowledges the LPDP Indonesia Endowment Fund for Education for a PhD Scholarship. G.F.T. acknowledges the Australian Government for the provision of an Australian Government Research Training Program (RTP) scholarship. S.A.M. acknowledges the support of the Australian Research Council (ARC) from a Future Fellowship (FT200100243) and Discovery Project (DP220103690). A.T.T. acknowledges the Engineering and Physical Sciences Research Council (EPSRC) for a Doctoral Training Grant (EP/N509462/1).

ABBREVIATIONS

Ph_7C_7H, *sym*-heptaphenylcycloheptatriene; **Ph_5C_5H**, *sym*-pentaphenylcyclopentadiene; DS, displaced-stacked

Additional references in the Supplementary Information.[72-81]

REFERENCES

1. Xie, Z.; C., C.; Xu, S.; Li, J.; Zhang, Y.; Liu, S.; Xu, J.; Chi, Z., White-Light Emission Strategy of a Single Organic Compound with Aggregation-Induced Emission and Delayed Fluorescence Properties. *Angew. Chem. Int. Ed.* **2015,** *54* (24), 7181-7184.
2. Geffroy, B.; le Roy, P.; Prat, C., Organic light-emitting diode (OLED) technology: materials, devices and display technologies. *Polym. Int.* **2006,** *55* (6), 572-582.
3. Moorthy, J. N.; Natrajan, P.; Venkatakrishnan, P.; Huang, D.-F.; Chow, T. J., Steric Inhibition of π-Stacking: 1,3,6,8-Tetraarylpyrenes as Efficient Blue Emitters in Organic Light Emitting Diodes (OLEDs). *Org. Lett.* **2007,** *9* (25), 5215-5218.
4. Cicoira, F.; Santato, C., Organic Light Emitting Field Effect Transistors: Advances and Perspectives. *Adv. Funct. Mater.* **2007,** *17* (17), 3421-3434.
5. Dickson, R. M.; Cubitt, A. B.; Tsien, R. Y.; Meorner, W. E., On/off blinking and switching behaviour of single molecules of green fluorescent protein. *Nature* **1997,** *388*, 355-358.
6. Li, H.; Wang, J.; Lin, H.; Xu, L.; Xu, W.; Wang, R.; Song, Y.; Zhu, D., Amplification of Fluorescent Contrast by Photonic Crystals in Optical Storage. *Adv. Mater.* **2010,** *22* (11), 1237-1241.
7. Ong, K.-H.; Liu, B., Applications of Fluorogens with Rotor Structures in Solar Cells. *Molecules* **2017,** *22* (6), 897.
8. Mei, J.; Leung, N. L. C.; Kwok, R. T. K.; Lam, J. W. Y.; Tang, B. Z., Aggregation-Induced Emission: Together We Shine, United We Soar! *Chem. Rev.* **2015,** *115* (21), 11718-11940.
9. Ma, S.; Du, S.; Pan, G.; Dai, S.; Xu, B.; Tian, W., Organic molecular aggregates: From aggregation structure to emission property. *Aggregate* **2021,** *2* (4), e96.
10. Zhang, H.; Zhao, Z.; Turley, A. T.; Wang, L.; McGonigal, P. R.; Tu, Y.; Li, W.; Wang, Z.; Kwok, R. T. K.; Lam, J. W. Y.; Tang, B. Z., Aggregate Science: From Structures to Properties. *Adv. Mater.* **2020,** *32* (36), 2001457.
11. Peng, Q.; Shuai, Z., Molecular mechanism of aggregation-induced emission. *Aggregate* **2021,** *2* (5), e91.
12. Li, Q.; Blancafort, L., A conical intersection model to explain aggregation induced emission in diphenyl dibenzofulvene. *Chem. Commun.* **2013,** *49*, 5966-5968.
13. Peng, X.-L.; Ruiz-Barragan, S.; Li, Z.-S.; Li, Q.-S.; Blancafort, L., Restricted access to a conical intersection to explain aggregation induced emission in dimethyl tetraphenylsilole. *J. Mater. Chem. C.* **2016,** *4*, 2802-2810.
14. Anthony, J. E., Functionalized Acenes and Heteroacenes for Organic Electronics. *Chem. Rev.* **2006,** *106* (12), 5028-5048.
15. Coropceanu, V.; Cornil, J.; da Silva Filho, D. A.; Olivier, Y.; Silbey, R.; Brédas, J.-L., Charge Transport in Organic Semiconductors. *Chem. Rev.* **2007,** *107* (4), 926-952.

16. Etherington, M. K.; Kukhta, N. A.; Higginbotham, H. F.; Danos, A.; Bismallah, A. N.; Graves, D. R.; McGonigal, P. R.; Haase, N.; Morherr, A.; Batsanov, A. S.; Pflumm, C.; Bhalla, V.; Bryce, M. R.; Monkman, A. P., Persistent Dimer Emission in Thermally Activated Delayed Fluorescence Materials. *J. Phys. Chem. C* **2019,** *123* (17), 11109-11117.
17. Etherington, M. K., Thermally Activated Delayed Fluorescence: Beyond the Single Molecule. *Front. Chem.* **2020,** *8*, 716.
18. Katrusiak, A., Lab in a DAC – high-pressure crystal chemistry in a diamond-anvil cell. *Acta Cryst. B* **2019,** *B75*, 918-926.
19. Marelli, E.; Casati, N.; Gozzo, F.; Macchi, P.; Simoncic, P.; Sironi, A., High pressure modification of organic NLO materials: large conformational re-arrangement of 4-aminobenzophenone. *CrystEngComm* **2011,** *13*, 6845-6849.
20. Li, N.; Liu, H.; Fang, Y.; Zhang, L.; Sui, L.; Yuan, K.; Wu, G.; Wang, K.; Yang, B.; Zou, B., Piezochromic luminescence behavior based on the molecular conformation change of nitro-triphenylamine *Appl. Phys. Lett.* **2022,** *121*, 111901.
21. Casati, N.; Macchi, P.; Sironi, A., Staggered to Eclipsed Conformational Rearrangement of [Co2(CO)6(PPh3)2] in the Solid State: An X-ray Diffraction Study at High Pressure and Low Temperature. *Angew. Chem. Int. Ed.* **2005,** *44* (47), 7736-7739.
22. Casati, N.; Macchi, P.; Sironi, A., Molecular Crystals Under High Pressure: Theoretical and Experimental Investigations of the Solid–Solid Phase Transitions in [Co2(CO)6(XPh3)2] (X=P, As). *Chem. Eur. J.* **2009,** *15* (17), 4446-4457.
23. Etcheverry-Berrios, A.; Parsons, S.; Kamenev, K. V.; Probert, M. R.; Moggach, S. A.; Murrie, M.; Brechin, E. K., Putting the Squeeze on Molecule-Based Magnets: Exploiting Pressure to Develop Magneto-Structural Correlations in Paramagnetic Coordination Compounds. *Magnetochemistry* **2020,** *6* (3), 32.
24. McKellar, S. C.; Moggach, S. A., Structural studies of metal–organic frameworks under high pressure. *Acta Cryst. B* **2015,** *B71*, 587-607.
25. Andrzejewski, M.; Katrusiak, A., Piezochromic Porous Metal–Organic Framework. *J. Phys. Chem. Lett.* **2017,** *8* (1), 279-284.
26. Andrzejewski, M.; Casati, N.; Katrusiak, A., Reversible pressure pre-amorphization of a piezochromic metal–organic framework. *Dalton Trans.* **2017,** *46*, 14795-14803.
27. Andrzejewski, M.; Katrusiak, A., Piezochromic Topology Switch in a Coordination Polymer. *J. Phys. Chem. Lett.* **2017,** *8* (5), 929-935.
28. Fang, J.; Fu, Z.; Chen, X.; Liu, Y.; Chen, F.; Wang, Y.; Li, H.; Yusran, Y.; Wang, K.; Valtchev, V.; Qui, S.; Zou, B.; Fang, Q., Piezochromism in Dynamic Three-Dimensional Covalent Organic Frameworks. *Angew. Chem. Int. Ed.* **2023,** *e202304234*.
29. Ma, Z.; Meng, X.; Ju, Y.; Li, A.; Qi, G.; Xu, W.; Zou, B.; Ma, Y.; Kuang, G.-C.; Jia, X., Pressure induced the largest emission wavelength change in a single crystal. *Dyes Pigm.* **2019,** *162*, 136-144.
30. Xiong, J.; Wang, K.; Yao, Z.; Zou, B.; Xu, J.; Bu, X.-H., Multi-Stimuli-Responsive Fluorescence Switching from a Pyridine-Functionalized Tetraphenylethene AIEgen. *ACS Appl. Mater. Interfaces* **2018,** *10* (6), 5819-5827.
31. Li, A.; Wang, J.; Xu, S.; Huo, Z.; Geng, Y.; xXu, W.; Cui, H., Distinct stimuli-responsive behavior for two polymorphs of 9,10-bis(phenylethynyl)anthracene under pressure based on intermolecular interactions. *Dyes Pigm.* **2019,** *170*, 107603.
32. Liu, Y.; Ye, Z.; Zhao, M.; Chen, Q.; Wang, Y.; Zhu, Q., Sensitive mechanofluorochromism based on conversion of paired and unpaired enantiomer packing modes. *Dyes Pigm.* **2017,** *145*, 391-398.
33. Jiang, M.; Gu, X.; Kwok, R. T. K.; Li, Y.; Sung, H. H. Y.; Zheng, X.; Zhang, Y.; Lam, J. W. Y.; Williams, I. D.; Huang, Z.; Wong, K. S.; Tang, B. Z., Mechanochromism: Multifunctional AIEgens: Ready Synthesis, Tunable Emission, Mechanochromism, Mitochondrial, and Bacterial Imaging. *Adv. Funct. Mater.* **2018,** *28* (1), 1870006.
34. Adil, L. R.; Iyer, P. K., Effects of incorporating regioisomers and flexible rotors to direct aggregation induced emission to achieve stimuli-responsive luminogens, security inks and chemical warfare agent sensors. *Chem. Commun.* **2020,** *56*, 7633-7636.
35. Sturala, J.; Etherington, M. K.; Bismallah, A. N.; Higginbotham, H. F.; Trewby, W.; Aguilar, J. A.; Bromley, E. H. C.; Avestro, A.-J.; Monkman, A. P.; McGonigal, P. R., Excited-State Aromatic Interactions in the Aggregation-Induced Emission of Molecular Rotors. *J. Am. Chem. Soc.* **2017,** *139* (49), 17882-17889.
36. Lee, E. C.; Kim, D.; Jurečka, p.; Tarakeshwar, P.; Hobza, P.; Kim, K. S., Understanding of Assembly Phenomena by Aromatic−Aromatic Interactions: Benzene Dimer and the Substituted Systems. *J. Phys. Chem. A* **2007,** *111* (18), 3446-3457.
37. Bludský, O.; Rubeš, m.; Soldán, p.; Nachtigall, P., Investigation of the benzene-dimer potential energy surface: DFT/CCSD(T) correction scheme. *J. Chem. Phys.* **2008,** *128* (11), 114102.
38. Ninković, D. B.; Filipović, J. P. B.; Hall, M. B.; Brothers, E. N.; Zarić, S. D., What Is Special about Aromatic–Aromatic Interactions? Significant Attraction at Large Horizontal Displacement. *ACS Central Sci.* **2020,** *6* (3), 420-425.
39. Martinez, C. R.; Iverson, B. L., Rethinking the term “pi-stacking”. *Chem. Sci.* **2012,** *3*, 2191-2201.
40. Turley, A. T.; Saha, P. K.; Danos, A.; Bismallah, A. N.; Monkman, A. P.; Yufit, D. S.; Curchod, B. F. E.; Etherington, M. K.; McGonigal, P. R., Extended Conjugation Attenuates the Quenching of Aggregation-Induced Emitters by Photocyclization Pathways. *Angew. Chem. Int. Ed.* **2022,** *61* (24), e202202193.
41. Saha, P. K.; Mallick, A.; Turley, A. T.; Bismallah, A. N.; Danos, A.; Monkman, A. P.; Avestro, A.-J.; Yufit, D. S.; McGonigal, P. R., Rupturing aromaticity by periphery overcrowding. *Nat. Chem.* **2023,** *15*, 516-525.
42. Chang, Z.-F.; Jing, L.-M.; Wei, C.; Dong, Y.-P.; Ye, Y.-C.; Zhao, Y. S.; Wang, J.-L., Hexaphenylbenzene-Based, π-Conjugated Snowflake-Shaped Luminophores: Tunable Aggregation-Induced Emission Effect and Piezofluorochromism. *Chem. Eur. J.* **2015,** *21* (23), 8504-8510.
43. Albrecht, K.; Matsuoka, K.; Fujita, K.; Yamaoto, K., Carbazole Dendrimers as Solution-Processable Thermally Activated Delayed-Fluorescence Materials. *Angew. Chem. Int. Ed.* **2015,** *54* (19), 5677-5682.

44. Li, Z.; Ye, S.; Liu, Y.; Yu, G.; Wu, W.; Qin, J.; Li, Z., New Hyperbranched Conjugated Polymers Containing Hexaphenylbenzene and Oxadiazole Units: Convenient Synthesis and Efficient Deep Blue Emitters for PLEDs Application. *J. Phys. Chem. B* **2010,** *114* (28), 9101-9108.
45. Yuan, H.; Wang, K.; Yang, K.; Liu, B.; Zou, B., Luminescence Properties of Compressed Tetraphenylethene: The Role of Intermolecular Interactions. *J. Phys. Chem. Lett.* **2014,** *5* (17), 2968-2973.
46. Wu, J.; Tang, J.; Wang, H.; Qi, Q.; Fang, X.; Liu, Y.; Xu, S.; Zhang, S. X.-A.; Zhang, H.; Xu, W., Reversible Piezofluorochromic Property and Intrinsic Structure Changes of Tetra(4-methoxyphenyl)ethylene under High Pressure. *J. Phys. Chem. A* **2015,** *119* (35), 9218-9224.
47. Man, T.; Xu, N.-S.; Yu, Z.-H.; Huo, Y.; Yuan, Y.; Shi, Z.-F.; Cao, X.-P.; Wang, L.; Zhang, H.-L., Modulation of piezochromic fluorescence behavior by subtle structural change. *Dyes Pigm.* **2019,** *166*, 301-306.
48. Feng, X.; Zhang, J.; Hu, Z.; Wang, Q.; Islam, M.; Ni, J.-S.; Elsegood, M. R. J.; Lam, J. W. Y.; Zhou, E.; Tang, B. Z., Pyrene-based aggregation-induced emission luminogens (AIEgen): structure correlated with particle size distribution and mechanochromism. *J. Mater. Chem. C.* **2019,** *7*, 6932-6940.
49. Yang, J.; Gao, X.; Xie, Z.; Gong, Y.; Fang, M.; Peng, Q.; Chi, Z.; Li, Z., Elucidating the Excited State of Mechanoluminescence in Organic Luminogens with Room-Temperature Phosphorescence. *Angew. Chem. Int. Ed.* **2017,** *56*, 15299-15303.
50. Li, A.; Liu, Y.; Han, L.; Xu, S.; Song, C.; Geng, Y.; Pan, L.; Xu, B.; Tiang, W.; Zhang, H.; Xu, W.; Cui, H., Pressure-induced remarkable luminescence-changing behaviours of 9, 10-distyrylanthracene and its derivatives with distinct substituents. *Dyes Pigm.* **2019,** *161*, 182-187.
51. Huang, G.; Jiang, Y.; Yang, S.; Li, B. S.; Tang, B. Z., Multistimuli Response and Polymorphism of a Novel Tetraphenylethylene Derivative. *Adv. Funct. Mater.* **2019,** *29* (16), 1900516.
52. Zhang, Y.; Zhuang, H.; Ouyang, M.; Hu, B.; Song, Q.; Sun, J.; Zhang, C.; Gu, C.; Xu, Y.; Ma, Y., Mechanochromic and thermochromic fluorescent properties of cyanostilbene derivatives. *Dyes Pigm.* **2013,** *98* (3), 486-492.
53. Gu, Y.; Liu, H.; Qui, R.; Liu, Z.; Wang, C.; Katsura, T.; Zhang, H.; Wu, M.; Yao, M.; Zheng, H.; Li, K.; Wang, y.; Wang, K.; Yang, B.; Ma, Y.; Zou, B., Pressure-Induced Emission Enhancement and Multicolor Emission for 1,2,3,4-Tetraphenyl-1,3-cyclopentadiene: Controlled Structure Evolution. *J. Phys. Chem. Lett.* **2019,** *10* (18), 5557-5562.
54. Li, N.; Gu, Y.; Chen, Y.; Zhang, L.; Zeng, Q.; Geng, T.; Wu, L.; Jiang, L.; Xio, G.; Wang, K.; Zou, B., Pressure-Induced Emission Enhancement and Piezochromism of Triphenylethylene. *J. Phys. Chem. C* **2019,** *123* (11), 6763-6767.
55. Tong, S.; Dai, J.; Sun, J.; Liu, Y.; Ma, X.; Liu, Z.; Ma, T.; Tan, J.; Yao, Z.; Wang, S.; Zheng, H.; Wang, K.; Hong, F.; Yu, X.; Gao, C.; Gu, X., Fluorescence-based monitoring of the pressure-induced aggregation microenvironment evolution for an AIEgen under multiple excitation channels. *Nat. Commun.* **2022,** *13* (1), 5234.
56. Gu, Y.; Sun, X.; Wu, M.; Wang, K., Pressure-shortened delayed fluorescence lifetime of solid-state thermally activated delayed fluorescent 4CzIPN: the structure evolution. *Phys. Chem. Chem. Phys.* **2023,** *Advance Article*.
57. Groom, C. R.; Bruno, I. J.; Lightfoot, M. P.; Ward, S. C., The Cambridge Structural Database. *Acta Cryst. B* **2016,** *B72*, 171-179.
58. Field, L. D.; Hambley, T. W.; Lindall, C. M.; Masters, A. F., Crystal and molecular structures of pentaphenylcyclopentadiene and of an isomer, 4,8-diphenyltribenzo[b,f,i]tricyclo[6.2.1.01,5]undecane, the product of a novel metal-assisted photoreaction. *Inorg. Chem.* **1992,** *31* (12), 2366-2370.
59. Miyazaki, M.; Fujii, M., Real time observation of the excimer formation dynamics of a gas phase benzene dimer by picosecond pump–probe spectroscopy. *Phys. Chem. Chem. Phys.* **2015,** *17*, 25989-5997.
60. Iyer, E. S. S.; Sadybekov, A.; Lioubashevski, O.; Krylov, A. I.; Ruhman, S., Rewriting the Story of Excimer Formation in Liquid Benzene. *J. Phys. Chem. A* **2017,** *121*, 1962-1975.
61. Konovalova, I. S.; Shishkina, S. V.; Bani-Khaled, G.; Muzyka, E. N.; Boyko, A. N., Intermolecular interactions in crystals of benzene and its mono- and dinitro derivatives: study from the energetic viewpoint. *CrystEngComm* **2019,** *21*, 2908-2919.
62. Gao, X.-C.; Cao, H.; Huang, L.; Huang, Y.-Y.; Zhang, B.-W.; Huang, C.-H., Comparison of the electroluminescence and its related properties of two cyclopentadiene derivatives. *Appl. Surf. Sci.* **2003,** *210* (3-4), 183-189.
63. Birks, J. B., Excimers. *Rep. Prog. Phys.* **1975,** *28*, 903-974.
64. Pensack, R. D.; Ashmore, R. J.; Paoletta, A. L.; Scholes, G. D., The Nature of Excimer Formation in Crystalline Pyrene Nanoparticles. *J. Phys. Chem. C* **2018,** *122* (36), 21004-21017.
65. Cliffe, M. J.; Goodwin, A. L., PASCal: a principal axis strain calculator for thermal expansion and compressibility determination. *J. Appl. Cryst.* **2012,** *45*, 1321-1329.
66. Huenerbein, R.; Grimme, S., Time-dependent density functional study of excimers and exciplexes of organic molecules. *Chem. Phys.* **2008,** *343* (2-3), 362-371.
67. Miyazaki, M.; Fujii, M., A structural study on the excimer state of an isolated benzene dimer using infrared spectroscopy in the skeletal vibration region. *Phys. Chem. Chem. Phys.* **2017,** *19*, 22759-22776.
68. Mackenzie, C. F.; Spackman, P. R.; Jayatilaka, D.; Spackman, M. A., CrystalExplorer model energies and energy frameworks: extension to metal coordination compounds, organic salts, solvates and open-shell systems. *IUCrJ* **2017,** *4*, 575-587.
69. Spackman, P. R.; Turner, M. J.; McKinnon, J. J.; Wolff, S. K.; Grimwood, D. J.; Jayatilaka, D.; Spackman, M. A., CrystalExplorer: a program for Hirshfeld surface analysis, visualization and quantitative analysis of molecular crystals. *J. Appl. Cryst.* **2021,** *54*, 1006-1011.
70. Jorgensen, W. I.; Severance, D. L., Aromatic-Aromatic Interactions: Free Energy Profiles for the Benzene Dimer in Water, Chloroform, and Liquid Benzene. *J. Am. Chem. Soc.* **1990,** *112*, 4768-4774.
71. Moellmann, J.; Grimme, S., Importance of London dispersion effects for the packing of molecular crystals: a case study for intramolecular stacking in a bis-thiophene derivative. *Phys. Chem. Chem. Phys.* **2010,** *12*, 8500-8504.

72. Agilent *CrysAlis Pro*, Agilent: Yarnton, England, 2009.
73. Sheldrick, G. M., SHELXT - Integrated space-group and crystal structure determination. *Acta Cryst. A* **2015,** *A71*, 3-8.
74. Sheldrick, G. M., Crystal structure refinement with SHELXL. *Acta Cryst. C* **2015,** *C71*, 3-8.
75. Dolomanov, O. V.; Bourhis, L. J.; Gildea, R. J.; Howard, J. A. K.; Puschmann, H., OLEX2: a complete structure solution, refinement and analysis program. *J. Appl. Cryst.* **2009,** *42*, 339-341.
76. Merrill, L.; Bassett, W. A., Miniature diamond anvil pressure cell for single crystal x-ray diffraction studies. Rev Sci Instrum 45, 290-294. *Rev. Sci. Instrum.* **1974,** *45*, 290-294.
77. Moggach, S. A.; Allan, D. R.; Parsons, S.; Warren, J. E., Incorporation of a new design of backing seat and anvil in a Merrill-Bassett diamond anvil cell. *J. Appl. Cryst.* **2008,** *41*, 249-251.
78. Piermarini, G. J.; Block, S.; Barnett, J. D.; Forman, R. A., Calibration of the pressure dependence of the R1 ruby fluorescence line to 195 kbar. *J. Appl. Phys.* **2008,** *46*, 2774-2780.
79. Spek, A. L., Single-crystal structure validation with the program PLATON. *J. Appl. Cryst.* **2003,** *36*, 7-13.
80. Macrae, C. F.; Bruno, I. J.; Chisholm, J. A.; Edginton, P. R.; McCabe, P.; Pidcock, E.; Rodriguez-Monge, L.; Taylor, R.; van de Streek, J.; Wood, P. A., Mercury CSD 2.0 - new features for the visualization and investigation of crystal structures. *J. Appl. Cryst.* **2008,** *41*, 466-470.
81. Gonzalez-Platas, J.; Alvaro, M.; Nestola, F.; Angel, R., EosFit7-GUI: a new graphical user interface for equation of state calculations, analyses and teaching. *J. Appl. Cryst.* **2016,** *49*, 1377-1382.